CrystEngComm

Accepted Manuscript

This article can be cited before page numbers have been issued, to do this please use: K. Chatzipanagis, M. Iafisco, T. Roncal-Herrero, M. Bilton, A. Tampieri, R. Kroger and J. M. Delgado-López, *CrystEngComm*, 2016, DOI: 10.1039/C6CE00521G.

ROYAL SOCIETY OF CHEMISTRY

www.rsc.org/crystengcomm

View Article Online
DOI: 10.1039/C6CE00521G

Crystallization of citrate-stabilized amorphous calcium phosphate to nanocrystalline apatite: a surface-mediated transformation

Received 00th January 20xx,
Accepted 00th January 20xx

DOI: 10.1039/x0xx00000x

www.rsc.org/

Konstantinos Chatzipanagis[a,§], Michele Iafisco[b,§], Teresa Roncal-Herrero[a], Matthew Bilton[a,c], Anna Tampieri[b], Roland Kröger[c,*] and José Manuel Delgado-López[d,*]

This work explores the mechanisms underlying the crystallization of citrate-functionalized amorphous calcium phosphate (cit-ACP) in two relevant media, combining *in situ* and *ex situ* characterization techniques. Results demonstrate that citrate desorption from cit-ACP triggers the surface-mediated transformation to nanocrystalline apatite (Ap). Our findings shed light on the key role of citrate, an important component of bone organic matrix, and the medium composition in controlling the rate of transformation and the morphology of the resulting Ap phase.

Many aspects of the mechanisms underlying the formation of nanocrystalline apatite (Ap), the main constituent of the inorganic phase of bone,[1, 2] remain under debate. In particular, the crystallization pathway, starting from an amorphous precursor and resulting in a well-defined mineral, is a matter of intensive research. [2-5] It has been previously demonstrated that in zebra fish bone[6] and in dental enamel[7] Ap formation does not occur directly by the association of ions from solution according to the classical nucleation and growth theory, but follows a "non-classical" crystallization pathway *via* an amorphous calcium phosphate (ACP) precursor. On this basis, the formation of ACP as a transient/intermediate phase is currently well accepted in *in vivo* bone mineralization.[8-11]

ACP crystallization in aqueous solutions has been largely studied revealing that factors such as pH, temperature and the presence of foreign ions (*e.g.* fluoride, magnesium, zinc, carbonates, and silicates) and additives (*e.g.* polyelectrolytes, phospholipids, polyglycols, proteins, etc.) affect the ACP stability and its transformation rate.[4, 5] This process has been proposed to occur, either directly from ACP to Ap or via the formation of intermediate CaP phases (mostly octacalcium phosphate; OCP), through different mechanisms:[4, 5] (i) dissolution-reprecipitation; (ii) clusters reorganization and, (iii) solution-mediated solid-solid transformation. Therefore, it seems reasonable to assume that several processes might occur even simultaneously.

In this context, the role of citrate in stabilizing the ACP has received less attention and only few reports can be found in the literature.[12-14] Citrate is an important component of mineralized tissues.[15] It accounts for ~2 wt% in bone,[16] which is a concentration approx. 5-25 times higher than that occurring in soft tissues. In fact, about 90% of the total citrate found in the body resides in bone.[15] In addition, recent NMR studies showed that it is strongly bound to the surface of bone Ap nanocrystals, controlling their shape and morphology.[17] However, its role in bone biomineralization is far from being clearly understood.

ACP not only plays a pivotal role in bone biomineralization but it is also widely used in medicine.[4] Hence, understanding its behaviour in aqueous media is of paramount importance for designing advanced biomaterials. However, *in situ* characterization of ACP is rarely found in literature likely due to the fact that it instantaneously transforms into a more stable crystalline phase and the difficulty of finding a suitable technique allowing for its characterization in solution.

This work explores the mechanisms underlying the crystallization of citrate-functionalized ACP (cit-ACP) immersed in two relevant media; pure water and the physiological phosphate-buffer saline (PBS) solution. The morphological evolution of cit-ACP in both aqueous solutions was studied by *ex situ* transmission electron microscopy (TEM), whereas the structural evolution was monitored by *in situ* time-resolved Raman spectroscopy.

Dry powder cit-ACP was synthesized by the batch precipitation method described elsewhere[12, 18, 19] (see electronic supplementary information, ESI, for further details). A negative zeta potential of -10.5 ± 3.9 mV was obtained for cit-ACP. This value is in excellent agreement with that obtained for citrate-stabilized ACP by Chen *et al.*[14] These authors related such a negative value to the adsorption of negatively charged citrate on ACP surface. However, further studies are necessary to confirm or exclude the possible presence of citrate also inside the ACP particles. Fig. 1A shows the Raman spectrum of cit-ACP particles (red line). It exhibits bands related to the OCO bending (845-847 cm^{-1}), OCO stretching (1400-1600 cm^{-1}) and CH_2 stretching (2928-2933 cm^{-1}) modes of citrate.[18] Fig. 1A also shows the Raman spectrum of the particles obtained after immersing cit-ACP in water for a total of 5 days (blue line). The same citrate vibrations are still noticeable. In addition, phosphate vibrational modes are clearly visible in both spectra. The assignments of the

[a] Department of Physics, University of York, York, United Kingdom.
[b] Institute of Science and Technology for Ceramics (ISTEC), National Research Council (CNR), Faenza, Italy
[c] Department of Chemistry, Simon Fraser University, Burnaby, Canada.
[d] Laboratorio de Estudios Cristalográficos, Instituto Andaluz de Ciencias de la Tierra (IACT, CSIC-UGR), Armilla, Granada, Spain.
(*) Corresponding authors: R. Kröger (roland.kroger@york.ac.uk) and J.M. Delgado-López (jmdl@iact.ugr.csic.es)
Electronic Supplementary Information (ESI) available: See DOI: 10.1039/x0xx00000x

View Article Online
DOI: 10.1039/C6CE00521G

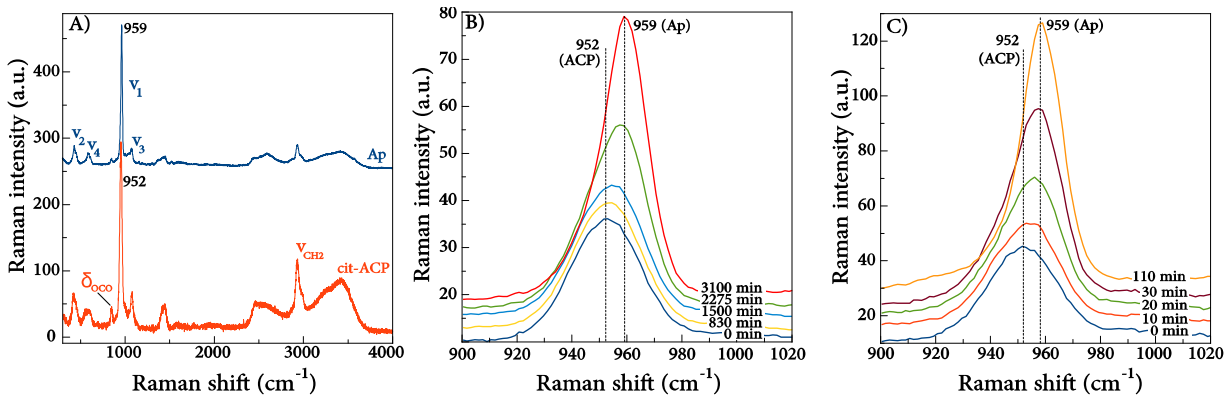

Figure 1. *(A) Raman spectra of dry cit-ACP (red line) and dry Ap (blue line, obtained after 5 days of cit-ACP immersion in water). The phosphate vibrational modes are denoted in blue whereas those involving bonds of citrate are marked in red. In situ time-dependent Raman spectra* (ν_1PO_4 vibrations) *collected during the transformation of cit-ACP in (B) water and in (C) PBS.*

corresponding vibrational modes are summarized in Table S1 (ESI). cit-ACP evolution was studied *in situ* by monitoring the symmetric vibration of phosphate groups (ν_1PO_4). In water (Fig. 1B), a single symmetric band centred at 952 cm^{-1}, assignable to ACP,[4, 20] is observed at the early stages. Upon maturation, this band progressively becomes asymmetric due to the formation of the crystalline Ap. Indeed, after 49 hours (2950 min), a distinct Raman peak at 959 cm^{-1} was observed. This value is in accordance with the Raman shift reported for Ap.[18, 21] *In situ* time-dependent Raman spectra of cit-ACP immersed in PBS (Fig. 1C) indicate that the cit-ACP-to-Ap conversion is greatly accelerated in this ionic medium.

The normalized ratio of the corresponding ν_1PO_4 Raman band of Ap and ACP (A_{959}/A_{952}, *i.e.* fraction of the transformed phase, Φ) (Fig. S1, ESI) was used to study the extent of the conversion in both media. The time dependence of Φ is represented in Fig. 2A. From these curves, we estimated an induction time in PBS of 10 minutes whereas the tapering off period was reached after 110 minutes. Conversely, the induction time in water was 830 minutes (*ca.* 14 hours), and the conversion gradually developed up to 3260 minutes (*ca.* 54 hours), when the steady state was achieved. Therefore, the appearance of Ap was significantly accelerated (by a factor of 75) in PBS.

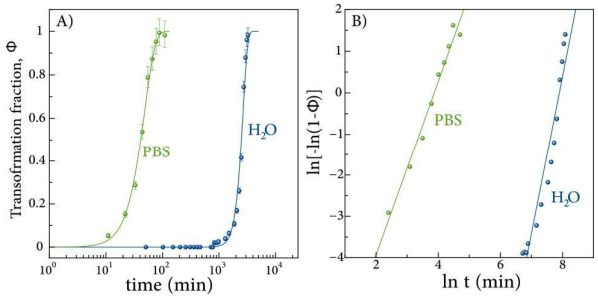

Figure 2. *A) Avrami fits to the data obtained for PBS and water. B) Plots of the linearized Avrami equation.*

The kinetics of the crystallization were studied in more detail using the Avrami model, which describes phase transformation in terms of volume fraction changes. This model is characterized by the generalized expression for the time dependence of the fraction of the transformed phase (Φ) as[22, 23]

$$\Phi = 1 - \exp\left(-kt^n\right)$$

where the parameter *k* entails information on nucleation density and growth rates whereas *n* represents the dimensionality of the growth and the possible impact of diffusion. We assume here that $A_{959(Ap)}/A_{952(cit\text{-}ACP)} \propto \Phi$ and upon complete transformation Φ=1, which means that the data were normalized. However, the data reveal that signal of $\nu_{1(cit\text{-}ACP)}$ never completely vanishes indicating that an amorphous/disordered layer remains at the crystallite surface even after full crystallization, as previously reported.[12, 13, 18, 24-26] The solid lines in Fig. 2A represent Avrami fits to the data. A plot of ln[-ln(1-Φ)] *vs* ln(t) as shown in Fig. 2B reveals how closely the transformation follows Avrami kinetics (in comparison to the straight line fits shown in the figure). Overall we observed an approximate - albeit not perfect - fit of the data to an Avrami type kinetics with a goodness of fit varying between 97% and 99%. Most notably, the transformation in PBS is indicative for an Avrami transformation. Whereas in water, the initial part of the curve shows a changing slope during the transformation. This indicates an enhanced role of a change of nucleation rates during the process. This difference can be explained by the approximations made in the Avrami equation, namely assuming spherical crystal growth and ignoring diffusion and a time dependence of the nucleation. The slope of the lines provides information on the parameter *n*, which differs significantly between the two cases. We find values of *n* = 2.1 and 3.8 for PBS and pure water, respectively. Assuming interface-controlled phase transformation Wong and Czernuszka[27] relate values of *n* above 3 to either zero nucleation (*n* = 3), decreasing

View Article Online
DOI: 10.1039/C6CE00521G

nucleation rate (n = 3-4), or constant nucleation rate (n = 4) for solvent mediated re-dissolution and re-crystallization processes. Values below 3 indicate diffusion-controlled growth. Therefore, in PBS our observations suggest a significant role of species diffusion in solution leading to a rapid crystal growth. To evaluate the corresponding transformation rates the time derivative of the Avrami-fit, namely $d\Phi(t)/dt$, was determined for cit-ACP transformation in the two media (Fig. S2C, ESI). This plot reveals a rapid transformation for pure PBS with a maximum transformation rate of 2.0 x 10^{-2} min^{-1}, which reduces to 1.2 x 10^{-3} min^{-1} for water. The significant difference in transformation rates is also reflected by the values for the parameter k, which are 9.4 x 10^{-14} min^{-n} for water and 2.9 x 10^{-4} min^{-n} for PBS. In our analysis we have assumed a single nucleation event but in particular for water it is highly likely that further nucleation events occur during the transformation affecting the value for k. As a control experiment, we also studied the impact of a PBS/water mixture (1:1 volume) on the transformation kinetics (Fig. S2, ESI). This revealed an intermediate timescale for full transformation between that of pure water and PBS.

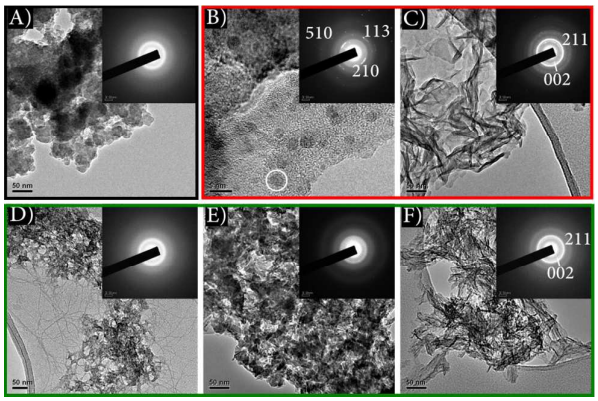

Figure 3. *(A) TEM micrograph and the corresponding SAED pattern of the as-prepared dry cit-ACP. (B-C, red square) Morphological evolution of the particles immersed in PBS (time: B, 10 min; C, 100 min) and (D-F, green square) water (time: D, 1 day: E, 2 days; F, 3 days). SAED pattern in B corresponds to the crystalline domains (dark spots, as the marked with the white circle). The scale bars correspond to 50 nm except for B, where is 5 nm.*

The morphological amorphous-to-crystalline evolution was studied *ex situ* by TEM. Fig. 3A shows TEM micrograph of the as-prepared cit-ACP nanoparticles and the corresponding selected area electron diffraction (SAED) pattern, which confirms their amorphous nature. The particles are aggregated exhibiting round shaped morphology with average diameters of *ca.* 50 nm, as previously reported.[12, 13] In PBS, after 10 min, which corresponds to the estimated induction time by Raman, formation of crystalline domains of about 3 nm in diameter within the aggregated cit-ACP particles were observed (Fig. 3B). The SAED pattern (insert in Fig. 3B) from these particles indicates that they are Ap (STM card file no. 09-432). Similar domains have been previously observed by high-resolution TEM during the ACP-to-Ap transformation,[28, 29] and has been proposed that Ap crystallization occurs from multiple nuclei within the ACP nanoparticles.[12, 28, 29] After 100 min (corresponding to the post-crystallization stage) platelet-like nanoparticles of Ap were observed which confirms that the transformation to Ap occurred (Fig. 3C). However, a different evolution was found in water. After one day (early stage of crystallization), the partial dissolution of ACP was observed (Fig. 3D) since amorphous particles appeared smaller than those shown in Fig. 3A. Subsequently, during the second day (intermediate stage of crystallization), we observed indistinctly either poorly crystalline aggregates providing very tenuous 002 reflections in the SAED pattern (Fig. 3E) or amorphous particles with diffuse borders (Fig. S3, ESI). Finally, after 3 days (corresponding to the post-crystallization stage) smaller Ap nanoparticles than those grown in PBS were observed (Fig. 3F).

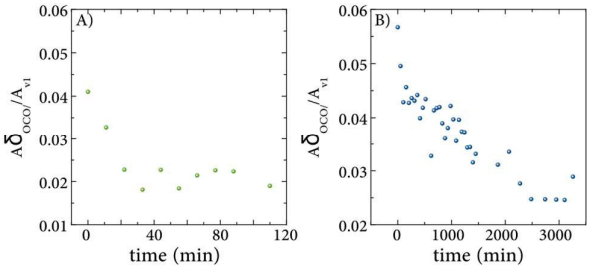

Figure 4. *Time-dependent evolution of the normalized peak of citrate ($A(\delta_{OCO})/A(v_1PO_4)$) in (A) PBS and (B) water.*

The large differences in the conversion kinetics of both media cannot be attributed to pH variations (Fig. S4, ESI). Actually, Boskey *et al.*[30] reported much lower differences between the conversion kinetic parameters at pH values similar to those measured in this work. The hydrolysis of ACP has been proposed to be the responsible for triggering its instantaneous crystallization to Ap in aqueous media.[31] However, in the case of cit-ACP, adsorbed citrate, blocking active sites, delays this transformation. In PBS, the citrate is rapidly released from the surface (Fig. 4A), most probably by ionic exchange with the phosphate of the medium,[32] which in turn reduces the ACP stability and increases the phosphate concentration within ACP. This leads to the rapid transformation to Ap, starting from small nuclei (as those appearing close to the surface in Fig. 3B). Conversely, a gradual release of citrate was found in water (Fig. 4B). After one day, when most of the citrate has been released, the partial dissolution of the ACP and the further re-crystallization of Ap occurred. However, the complete dissolution of cit-ACP can be excluded as suggested by the time-lapse video recorded during the transformation (movie S1, ESI).

View Article Online
DOI: 10.1039/C6CE00521G

Conclusions

The combination of *ex situ* (TEM and SAED) and *in situ* (time-dependent Raman spectroscopy) experiments allowed for monitoring the crystallization of cit-ACP in two relevant media; *i.e.* ultrapure water and PBS. Results demonstrate that cit-ACP directly transforms to Ap without involving the formation of any other intermediate calcium phosphate phase. Citrate desorption from ACP triggers the Ap crystallization, which occurs through a surface-mediated process. This process involves the ionic-exchange between labile ions from the surface of cit-ACP nanoparticles and ionic species in solution. The exchange between adsorbed citrate and phosphate promotes the rapid Ap crystallization in PBS. Indeed, the presence of phosphates in the media greatly accelerates such conversion (by a factor of 75) as determined by *in situ* Raman. Overall, our results highlight two important aspects of cit-ACP to Ap transformation: the role of citrate (or analogous organic additives) in stabilizing ACP and preventing the instantaneous transformation, and the impact of ionic species concentration (*e.g.*, phosphate) in controlling crystallization rates and mechanisms. These aspects are highly relevant for gaining a better understanding in bone biomineralization process and for designing advanced biomaterials.

Notes and references

§ Both authors equally contributed to this work.

This work has been carried out in the framework of the projects SMILEY (FP7-NMP-2012-SMALL-6-310637), BioBone (Andalucía Talent Hub, co-funded by Junta de Andalucía and EU-FP7 within the Marie-Curie Actions), the UK Engineering and Physical Sciences Research Council (EPSRC) (Grant No. EP/I001514/1), funding the Material Interface with Biology (MIB) consortium, and the short-term mobility program (STM 2015) from the National Research Council of Italy (CNR) for J.M.D.-L. We would like also to thank York JEOL Nanocentre for the use of their facilities.

1. H. A. Lowenstam and S. Weiner, *On Biomineralization*, University Press, Oxford, 1989.
2. J. Gómez-Morales, M. Iafisco, J. M. Delgado-López, S. Sarda and C. Drouet, *Prog. Cryst. Growth Ch.*, 2013, **59**, 1-46.
3. H. Pan, X. Y. Liu, R. Tang and H. Y. Xu, *Chem. Commun.*, 2010, **46**, 7415-7417.
4. C. Combes and C. Rey, *Acta Biomater.*, 2010, **6**, 3362-3378.
5. S. V. Dorozhkin, *Acta Biomater.*, 2010, **6**, 4457-4475.
6. J. Mahamid, B. Aichmayer, E. Shimoni, R. Ziblat, C. Li, S. Siegel, O. Paris, P. Fratzl, S. Weiner and L. Addadi, *Proc. Natl. Acad. Sci. USA*, 2010, **107**, 6316-6321.
7. E. Beniash, R. A. Metzler, R. S. K. Lam and P. U. P. A. Gilbert, *J. Struct. Biol.*, 2009, **166**, 133-143.
8. M. J. Olszta, X. Cheng, S. S. Jee, R. Kumar, Y.-Y. Kim, M. J. Kaufman, E. P. Douglas and L. B. Gower, *Mater. Sci. Eng. R*, 2007, **58**, 77-116.
9. L. B. Gower, *Chem. Rev.*, 2008, **108**, 4551-4627.
10. S. Weiner, J. Mahamid, Y. Politi, Y. Ma and L. Addadi, *Front. Mater. Sci. China*, 2009, **3**, 104-108.
11. F. Nudelman, K. Pieterse, A. George, P. H. H. Bomans, H. Friedrich, L. J. Brylka, P. A. J. Hilbers, G. de With and N. Sommerdijk, *Nat. Mater.*, 2010, **9**, 1004-1009.
12. J. M. Delgado-López, R. Frison, A. Cervellino, J. Gómez-Morales, A. Guagliardi and N. Masciocchi, *Adv. Funct. Mater.*, 2014, **24**, 1090-1099.
13. M. Iafisco, G. B. Ramirez-Rodriguez, Y. Sakhno, A. Tampieri, G. Martra, J. Gomez-Morales and J. M. Delgado-Lopez, *CrystEngComm*, 2015, **17**, 507-511.
14. Y. Chen, W. Gu, H. Pan, S. Jiang and R. Tang, *CrystEngComm*, 2014, **16**, 1864-1867.
15. R. L. Hartles, *Adv. Oral Biol.*, 1964, **1**, 225-253
16. E. Davies, K. H. Müller, W. C. Wong, C. J. Pickard, D. G. Reid, J. N. Skepper and M. J. Duer, *Proc. Natl. Acad. Sci. USA*, 2014, **111**, E1354-E1363.
17. Y. Y. Hu, A. Rawal and K. Schmidt-Rohr, *Proc. Natl. Acad. Sci. USA*, 2010, **107**, 22425-22429.
18. J. M. Delgado-López, M. Iafisco, I. Rodríguez, A. Tampieri, M. Prat and J. Gómez-Morales, *Acta Biomater.*, 2012, **8**, 3491-3499.
19. A. López-Macipe, J. Gómez-Morales and R. Rodríguez-Clemente, *Adv. Mater.*, 1998, **10**, 49.
20. G. B. Ramírez-Rodríguez, J. M. Delgado-López and J. Gómez-Morales, *CrystEngComm*, 2013, **15**, 2206-2212.
21. C. P. Tarnowski, M. A. Ignelzi and M. D. Morris, *J. Bone Miner. Res.*, 2002, **17**, 1118-1126.
22. M. Avrami, *J. Chem. Phys.*, 1941, **9**, 177-184.
23. M. C. Weinberg, D. P. Birnie Iii and V. A. Shneidman, *J. Non-Cryst. Solids*, 1997, **219**, 89-99.
24. Y. Sakhno, L. Bertinetti, M. Iafisco, A. Tampieri, N. Roveri and G. Martra, *J. Phys. Chem. C*, 2010, **114**, 16640-16648.
25. Y. Wang, S. Von Euw, F. M. Fernandes, S. Cassaignon, M. Selmane, G. Laurent, G. Pehau-Arnaudet, C. Coelho, L. Bonhomme-Coury, M.-M. Giraud-Guille, F. Babonneau, T. Azaïs and N. Nassif, *Nat. Mater.*, 2013, **12**, 1144-1153.
26. M. Duer and A. Veis, *Nat. Mater.*, 2013, **12**, 1081-1082.
27. A. T. C. Wong and J. T. Czernuszka, *Colloids Surf. A*, 1993, **78**, 245-253.
28. C.-G. Wang, J.-W. Liao, B.-D. Gou, J. Huang, R.-K. Tang, J.-H. Tao, T.-L. Zhang and K. Wang, *Cryst. Growth Des.*, 2009, **9**, 2620-2626.
29. B. Xie, T. J. Halter, B. M. Borah and G. H. Nancollas, *Cryst. Growth Des.*, 2014, **14**, 1659-1665.
30. A. L. Boskey and A. S. Posner, *J. Phys. Chem.*, 1973, **77**, 2313-2317.
31. S. Somrani, M. Banu, M. Jemal and C. Rey, *J. Solid State Chem.*, 2005, **178**, 1337-1348.
32. C. Rey, C. Combes, C. Drouet, S. Cazalbou, D. Grossin, F. Brouillet and S. Sarda, *Prog. Cryst. Growth Ch.*, 2014, **60**, 63-73.

View Article Online
DOI: 10.1039/C6CE00521G

Graphical abstract

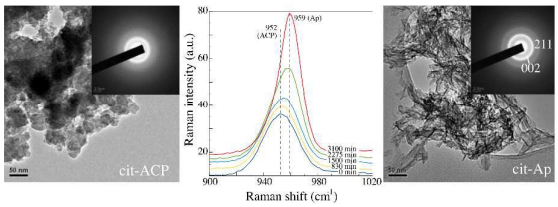

The mechanisms underlying the crystallization of citrate-functionalized amorphous calcium phosphate (cit-ACP) in two relevant media (water and PBS) have been explored by combining *in situ* Raman spectroscopy and *ex situ* TEM. Citrate desorption from cit-ACP triggers the surface-mediated crystallization to nanocrystalline apatite (cit-Ap).